

Optical spectroscopy of the blue supergiant Sk–69° 279 and its circumstellar shell with SALT

V. V. Gvaramadze,^{1,2,3*} A. Y. Kniazev,^{1,4,5} O. V. Maryeva,^{6,7}
and L. N. Berdnikov^{1,3,8}

¹*Sternberg Astronomical Institute, Lomonosov Moscow State University, Universitetskij Pr. 13, Moscow 119992, Russia*

²*Space Research Institute, Russian Academy of Sciences, Profsoyuznaya 84/32, 117997 Moscow, Russia*

³*Isaac Newton Institute of Chile, Moscow Branch, Universitetskij Pr. 13, Moscow 119992, Russia*

⁴*South African Astronomical Observatory, PO Box 9, 7935 Observatory, Cape Town, South Africa*

⁵*Southern African Large Telescope Foundation, PO Box 9, 7935 Observatory, Cape Town, South Africa*

⁶*Astronomical Institute, Czech Academy of Sciences, Fričova 298, 251 65 Ondřejov, Czech Republic*

⁷*Special Astrophysical Observatory of the Russian Academy of Sciences, Nizhnii Arkhyz, 369167, Russia*

⁸*Astronomy and Astrophysics Research Division, Entoto Observatory and Research Center, PO Box 8412, Addis Ababa, Ethiopia*

Accepted 2017 October 31. Received 2017 October 31; in original form 2017 September 23

ABSTRACT

We report the results of optical spectroscopy of the blue supergiant Sk–69° 279 and its circular shell in the Large Magellanic Cloud (LMC) with the Southern African Large Telescope (SALT). We classify Sk–69° 279 as an O9.2Iaf star and analyse its spectrum by using the stellar atmosphere code CMFGEN, obtaining a stellar temperature of ≈ 30 kK, a luminosity of $\log(L_*/L_\odot) = 5.54$, a mass-loss rate of $\log(\dot{M}/M_\odot \text{ yr}^{-1}) = -5.26$, and a wind velocity of 800 km s^{-1} . We found also that Sk–69° 279 possesses an extended atmosphere with an effective temperature of ≈ 24 kK and that its surface helium and nitrogen abundances are enhanced, respectively, by factors of ≈ 2 and 20–30. This suggests that either Sk–69° 279 was initially a (single) fast-rotating ($\gtrsim 400 \text{ km s}^{-1}$) star, which only recently evolved off the main sequence, or that it is a product of close binary evolution. The long-slit spectroscopy of the shell around Sk–69° 279 revealed that its nitrogen abundance is enhanced by the same factor as the stellar atmosphere, which implies that the shell is composed mostly of the CNO processed material lost by the star. Our findings support previous propositions that some massive stars can produce compact circumstellar shells and, presumably, appear as luminous blue variables while they are still on the main sequence or have only recently left it.

Key words: circumstellar matter – stars: emission-line, Be – stars: fundamental parameters – stars: individual: Sk–69° 279 – stars: massive – supergiants

1 INTRODUCTION

Mass loss from massive stars results (under proper conditions) in the formation of compact (pc-scale) circumstellar nebulae of various morphologies. Detection of CNO processed material in some of these nebulae by means of spectroscopic observations might indicate that their associated stars are at advanced stages of evolution, although it is also possible that massive stars can eject nebulae while they are relatively unevolved, i.e. still on the main sequence (e.g. Lamers et al. 2001). Among the massive stars, the compact circumstellar nebulae are most often found around lu-

minous blue variables (LBVs). Namely, observations show that about 60 per cent of known bona fide and candidate LBVs are surrounded by such nebulae (Nota et al. 1995; Clark, Larionov & Arkharov 2005). This is contrasted by the detection of only a few circumstellar nebulae around Wolf-Rayet (e.g. Marston 1995) and other types of evolved massive stars, and suggests that the duration of the LBV phase is comparable to the lifetime of their circumstellar nebulae ($\sim 10^4$ yr) and is much shorter than that of other major evolutionary phases in the life of massive stars.

A detection of compact nebulae can be considered as an indication that their associated stars are massive and (presumably) evolved (e.g. Clark et al. 2003). Indeed, untargeted searches for compact infrared nebulae in the archival

* E-mail: vgvaram@mx.iki.rssi.ru

data of the *Spitzer Space Telescope* and the *Wide-field Infrared Survey Explorer* (e.g. Gvaramadze, Kniazev & Fabrika 2010; Wachter et al. 2010; Gvaramadze et al. 2012a) led to the discovery of many dozens of such stars, of which, as expected, the most numerous are LBV-like stars (Kniazev & Gvaramadze 2015; Gvaramadze & Kniazev 2017, and references therein). With newly detected candidate and bona fide LBVs, the percentage of these stars with circumstellar nebulae has increased to more than 70 per cent (Kniazev, Gvaramadze & Berdnikov 2015; Gvaramadze & Kniazev 2017).

The presence of compact nebulae around hot, luminous (non-Wolf-Rayet) stars could be used to consider them as ex-/dormant LBVs even if they currently do not show significant spectroscopic and photometric variability (e.g. Bohannan 1997). On the other hand, it is still not fully clear at what point(s) in the evolution the massive stars become LBVs and produce their nebulae. Although it is likely that many LBVs are at advanced stages of stellar evolution, there are also observational hints that the LBV phenomenon might be related to stars which only recently left the main sequence or even still on it, and that the LBV-like nebulae might be ejected *before* their underlying stars become LBVs (Lamers et al. 2001). A possible example of such a star – the blue supergiant Sk–69° 279 in the Large Magellanic Cloud (LMC) – is the subject of this paper.

In Section 2, we present Sk–69° 279 and its circumstellar shell. Section 3 describes our spectroscopic and photometric observations. The spectral classification of Sk–69° 279 and the results of modelling of its spectrum with the stellar atmosphere code *CMFGEN* are given, respectively, in Sections 4.1 and 4.2. Spectroscopy of the circumstellar shell is discussed in Section 5. In Section 6, we discuss the obtained results and some issues related to the content of the paper.

2 SK–69° 279 AND ITS CIRCUMSTELLAR SHELL

Sk–69° 279 was identified as an OB star by Sanduleak (1970) using an objective prism survey for LMC members. Bohannan & Epps (1974) found in the objective prism spectrum of this star (object #619 in their survey of H α emission-line stars in the LMC) the H α emission line and an unspecified sharp emission feature bluewards of this line. Later on, Rousseau et al. (1978) classified Sk–69° 279 as O–B0 (also based on an objective prism spectrum), while Conti, Garmany & Massey (1986) refined the spectral type of this star to O9f using slit spectroscopy. Smith Neubig & Bruhweiler (1999) classified Sk–69° 279 as a B0 II star using its *International Ultraviolet Explorer* (*IUE*) spectrum. This classification was indicated as tentative (i.e. B0 II:) because the luminosity class assigned by the ultraviolet (UV) spectral features does not agree with that implied by the derived absolute magnitude. Also, Smith Neubig & Bruhweiler (1999) found that the B star luminosity indicators – the Si IV, C IV, Al III and Fe III lines – are weak in the spectrum of Sk–69° 279, which is a characteristic of most confirmed and candidate LBVs in their data set. The LBV nature of Sk–69° 279 is also suggested by the presence of a circular shell of CNO processed material around this star (Weis et al. 1997). But since the star does not show significant pho-

tometric variability, at least during the last decades, it was considered as an ex-/dormant LBV in the comprehensive study of LBVs in the Milky Way and Magellanic Clouds by van Genderen (2000; see also Section 3.2).

The circular shell around Sk–69° 279 was discovered by Weis et al. (1995) using narrow-band imaging in H α . In the discovery image, it appears as a complete circular shell with a diameter of 18 arcsec, which at a distance to the LMC of 50 kpc (Gibson 2000) corresponds to a linear size of ≈ 4.4 pc. Échelle spectroscopy of the shell revealed a high [N II] $\lambda 6584$ /H α ratio (a factor of 10 higher than in the background H II region), which was interpreted as an indication that the shell is composed of stellar material (Weis et al. 1997). It was also found that the shell expands with a velocity of 14 km s $^{-1}$ and that the systemic velocity of the shell of 230 km s $^{-1}$ is offset by 20 km s $^{-1}$ with respect to the local medium (Weis et al. 1997).

The mid-infrared counterpart of the shell around Sk–69° 279 was discovered during our search for bow shocks generated by runaway massive stars in the Magellanic Clouds using the *Spitzer Space Telescope* Legacy Survey called “Surveying the Agents of a Galaxy’s Evolution” (SAGE¹; Meixner et al. 2006) (for motivation and some results of this search, see Gvaramadze, Kroupa & Pflamm-Altenburg 2010 and Gvaramadze, Pflamm-Altenburg & Kroupa 2011). The survey provides 3.6, 4.5, 5.8 and 8.0 μ m images obtained with the Infrared Array Camera (IRAC; Fazio et al. 2004) and 24, 70 and 160 μ m images obtained with the Multiband Imaging Photometer for *Spitzer* (MIPS; Rieke et al. 2004). Besides detection of bow shocks, we discovered in the LMC two circular shells of almost the same angular size, one of which turns out to be associated with the already known optical nebula produced by Sk–69° 279 (Weis et al. 1995), while the second one was previously unknown².

Fig. 1 shows *Herschel* Space Observatory (Pilbratt et al. 2010) 250 and 160 μ m, *Spitzer* MIPS 70 and 24 μ m and IRAC 8 μ m, and Digitized Sky Survey II (DSS-II; McLean et al. 2000) red band images of Sk–69° 279 (indicated by a circle) and its circular shell. The shell is clearly seen in the 24 μ m image as a circular nebula of the same angular diameter as the optical one (i.e. ≈ 18 arcsec) with the northern edge somewhat brighter than the opposite one. The brightness asymmetry could be understood if the more brighter side of the shell impinges on a more denser ambient medium, as is evidenced by the presence of diffuse emission in the north direction attached to the shell in the *Herschel* 160 μ m and *Spitzer* 70 and 8 μ m images, or might be caused by stellar motion in the north direction (cf. Section 6). Fig. 1 also shows that there is a gleam of emission associated with the shell in the *Spitzer* 8 μ m and DSS-II images.

The details of Sk–69° 279 are summarized in Table 1. The spectral type is based on our spectroscopic observations (see Section 4.1). The *U* magnitude is from Zaritsky

¹ <http://sage.stsci.edu/>

² Follow-up spectroscopy of this shell showed that it is composed of unprocessed material, while spectroscopy of its central stars led to the discovery of a WN3b star in a binary system with an O6 V star and a separate B0 V star, which hints at the possibility that these stars are members of a previously unrecognized star cluster (Gvaramadze et al. 2014b).

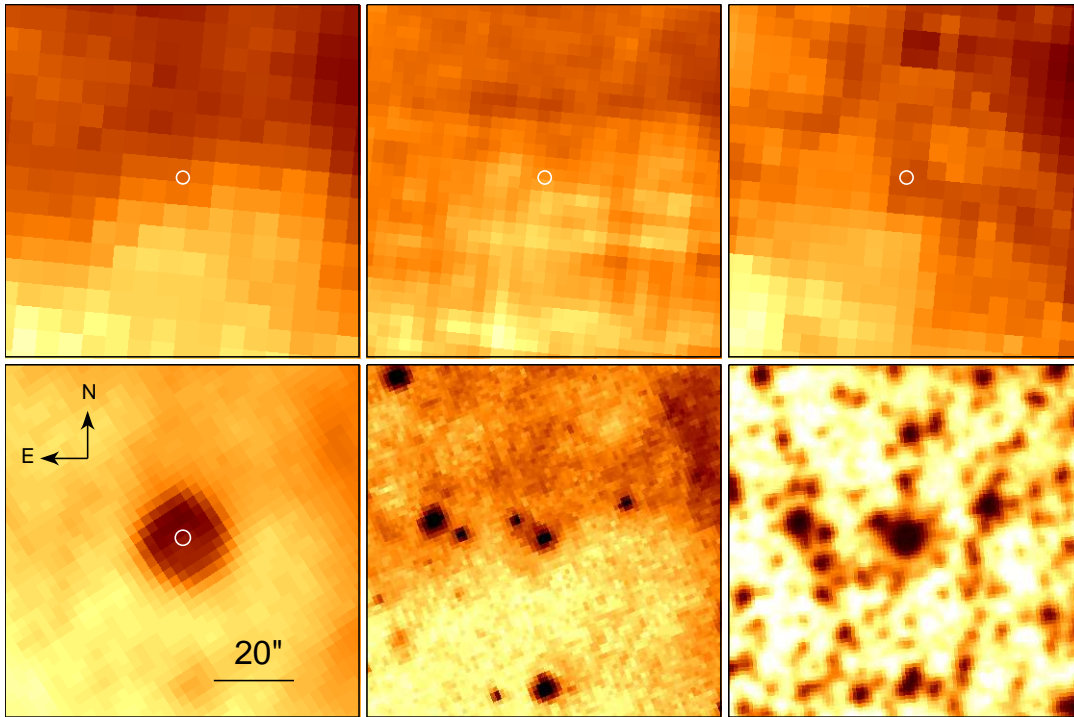


Figure 1. From left to right, and from top to bottom: *Herschel* 250 and 160 μm , *Spitzer* 70, 24 and 8 μm , and DSS-II red-band images of the region of the LMC containing Sk-69° 279 (indicated by a circle) and its circular shell. The orientation and the scale of the images are the same. At the distance of the LMC of 50 kpc, 20 arcsec corresponds to ≈ 4.8 pc.

Table 1. Details of Sk-69° 279.

| | |
|----------------------------|---|
| Spectral type | O9.2 Iaf |
| RA(J2000) | 05 ^h 41 ^m 44 ^s .67 |
| Dec(J2000) | -69° 35' 15".0 |
| <i>U</i> (mag) | 12.08±0.02 |
| <i>B</i> (mag) | 12.87±0.01 |
| <i>V</i> (mag) | 12.81±0.01 |
| <i>I_c</i> (mag) | 12.69±0.01 |
| <i>J</i> (mag) | 12.678±0.029 |
| <i>H</i> (mag) | 12.583±0.037 |
| <i>K_s</i> (mag) | 12.528±0.038 |
| [3.6] (mag) | 12.286±0.028 |
| [4.5] (mag) | 12.129±0.029 |
| [5.8] (mag) | 12.082±0.043 |
| [8.0] (mag) | 11.829±0.041 |

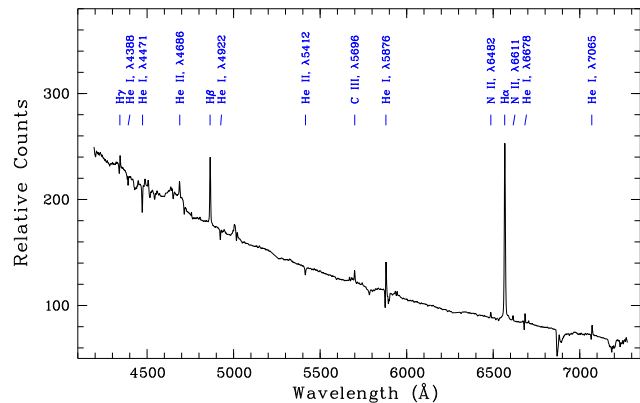


Figure 2. The fully reduced 1D RSS spectrum of Sk-69° 279 with the most prominent lines indicated.

3 OBSERVATIONS OF SK-69° 279 AND ITS CIRCUMSTELLAR SHELL

3.1 Spectroscopy

et al (2004). The BVI_c magnitudes are the mean values derived from our three CCD measurements in 2013–2016 (see Table 3). The coordinates and the JHK_s photometry are taken from the Two-Micron All Sky Survey (2MASS) All-Sky Catalog of Point Sources (Cutri et al. 2003). The IRAC ([3.6]–[8.0]) photometry is from Bonanos et al. (2009).

Sk-69° 279 and its circumstellar shell were observed on 2012 February 20 with the Southern African Large Telescope (SALT; Buckley, Swart & Meiring 2006; O’Donoghue et al. 2006) using the Robert Stobie Spectrograph (RSS; Burgh et al. 2003; Kobulnicky et al. 2003) in the long-slit mode with a 1.25 arcsec slit width. The slit was oriented in the north-south direction, i.e. at a position angle (PA) of

PA=0°. The PG900 grating was used to cover the spectral range of 4200–7400 Å with a final reciprocal dispersion of 0.97 Å pixel⁻¹. The spectral resolution full width at half-maximum (FWHM) is 4.45±0.15 Å. The total exposure time was 300 s. An Xe lamp arc spectrum was taken immediately after the science frames. Spectrophotometric standard stars were observed during twilight time for the relative flux calibration. Absolute flux calibration is not feasible with SALT because the unfilled entrance pupil of the telescope moves during the observations. Still, we were able to calibrate the spectrum by adjusting its *V* band flux to the mean *V* magnitude of the star of 12.81 (see Section 3.2) using programs described in Kniazev et al. (2005). Primary reduction of the data was done in the standard way with the SALT science pipeline (Crawford et al. 2010). Following long-slit data reduction was carried out in the way described in Kniazev et al. (2008). The resulting reduced RSS spectrum is shown in Fig. 2.

For spectral modelling, to search for possible spectral variability and to derive the rotational velocity, we obtained high-resolution spectra of Sk–69° 279 with the SALT High Resolution Spectrograph (HRS; Barnes et al. 2008; Bramall et al. 2010; Bramall et al. 2012; Crause et al. 2014) – a dual-beam, fibre-fed échelle spectrograph. The data were taken on 2016 October 27 and 2017 September 26 in the low-resolution (LR) mode of HRS. The spectra cover a spectral range of 3800–9000 Å at a resolution of $R = 16\,000$. The exposure time in each observation was 3000 s. Primary reduction of the HRS data was done using the SALT science pipeline (Crawford et al. 2010), which includes over-scan and gain corrections, and bias subtraction. The rest of the reduction was done using the MIDAS pipeline as described in detail in Kniazev, Gvaramadze & Berdnikov (2016). Equivalent widths (EWs), FWHMs and heliocentric radial velocities (RVs) of some lines in the 2016’s HRS spectrum (measured applying the MIDAS programs; see Kniazev et al. 2004 for details) are given in Table 2.

To investigate Sk–69° 279 in the UV range, we retrieved its spectra, obtained with the Cosmic Origins Spectrograph (COS) on board the *Hubble Space Telescope* (HST), from the Mikulski Archive for Space Telescopes (MAST)³. The spectra were obtained with the G130M and G160M gratings covering the spectral range from 1170 to 1770 Å with a resolution of $R = 16\,000 - 21\,000$.

3.2 Photometry

To search for possible photometric variability of Sk–69° 279, we determined its *B*, *V* and *I_c* magnitudes on CCD frames obtained with the 76-cm telescope of the South African Astronomical Observatory during our three observing runs in 2013–2016. We used an SBIG ST-10XME CCD camera equipped with *BVI_c* filters of the Kron-Cousins system (see e.g. Berdnikov et al. 2012). The resulting photometry is presented in Table 3. From table it follows that Sk–69° 279 did not experience major changes in its brightness during the three years: its *B*, *V* and *I_c* magnitudes remained almost constant with mean values of 12.87±0.01, 12.81±0.01 and 12.69±0.01 mag, respectively. The *V* magnitude and the

Table 2. EWs, FWHMs and RVs of some lines in the 2016’s HRS spectrum of Sk–69° 279. RVs of lines noticeably affected by P Cygni absorptions are starred.

| λ_0 (Å) Ion | EW(λ) (Å) | FWHM(λ) (Å) | RV (km s ⁻¹) |
|---------------------|---------------------|-----------------------|--------------------------|
| 4026 He I | -0.590±0.010 | 2.489± 0.044 | 185.08±0.91 |
| 4089 Si IV | -0.540±0.006 | 1.512± 0.017 | 224.05±0.68 |
| 4144 He I | -0.150±0.006 | 1.572± 0.058 | 224.95±0.66 |
| 4200 He II | -0.140±0.005 | 2.336± 0.056 | 236.94±0.61 |
| 4340 H γ | 0.316±0.017 | 1.097± 0.067 | 238.44±2.04* |
| 4379 N III | -0.040±0.004 | 1.149± 0.089 | 243.84±0.55 |
| 4388 He I | -0.240±0.005 | 1.946± 0.032 | 212.36±0.59 |
| 4471 He I | -0.600±0.010 | 2.928± 0.053 | 140.41±0.84* |
| 4485 S IV | 0.140±0.004 | 1.522± 0.025 | 233.95±0.85 |
| 4504 S IV | 0.190±0.004 | 1.568± 0.026 | 235.45±0.87 |
| 4541 He II | -0.190±0.005 | 2.163± 0.035 | 238.44±0.56 |
| 4686 He II | 0.230±0.006 | 4.047± 0.117 | 197.67±3.11 |
| 4713 He I | -0.150±0.008 | 1.758± 0.098 | 224.05±0.68 |
| 4861 H β | 2.185±0.023 | 2.301± 0.027 | 236.04±0.83* |
| 4922 He I | -0.260±0.007 | 2.843± 0.073 | 185.98±0.62* |
| 5016 He I | -0.100±0.005 | 2.399± 0.099 | 81.95±0.51* |
| 5412 He II | -0.230±0.006 | 2.554± 0.047 | 237.84±0.50 |
| 5696 C III | 0.380±0.005 | 1.736± 0.013 | 227.35±0.48 |
| 5876 He I | 1.373±0.066 | 2.201± 0.122 | 270.52±2.68* |
| 6482 N II | 0.249±0.006 | 1.704± 0.039 | 218.96±0.82 |
| 6563 H α | 2.449±0.055 | 4.546± 0.023 | 239.94±0.55 |
| 6611 N II | 0.319±0.005 | 1.779± 0.023 | 218.96±0.54 |
| 6678 He I | 0.590±0.020 | 1.816± 0.068 | 245.94±1.34* |
| 6703 Si IV | 0.101±0.004 | 1.625± 0.031 | 163.19±0.66 |
| 7065 He I | 0.638±0.020 | 1.957± 0.071 | 236.64±1.31* |
| 8502 P16 | -0.430±0.009 | 6.024± 0.113 | 209.66±0.41 |
| 8545 P15 | -0.410±0.018 | 5.725± 0.272 | 221.65±0.67 |
| 8598 P14 | -0.510±0.008 | 5.716± 0.064 | 222.25±0.36 |
| 8665 P13 | -0.700±0.010 | 5.880± 0.067 | 228.25±0.41 |
| 8750 P12 | -0.750±0.012 | 6.299± 0.101 | 221.05±0.48 |

Table 3. Photometry of Sk–69° 279.

| Date | <i>B</i> | <i>V</i> | <i>I_c</i> |
|----------------|------------|------------|----------------------|
| 2013 January 3 | 12.86±0.01 | 12.81±0.01 | 12.67±0.01 |
| 2014 April 5 | 12.92±0.02 | 12.83±0.01 | 12.75±0.01 |
| 2016 March 24 | 12.82±0.01 | 12.79±0.01 | 12.66±0.01 |

mean value of the *B* – *V* colour of 0.06±0.01 are in good agreement with the values measured for Sk–69° 279 by Isersstedt (1975), respectively, 12.79 and 0.05 mag.

Also, we used data from the archives of the Digital Access to a Sky Century @ Harvard (DASCH; Grindlay et al. 2009) project, the All-Sky Automated Survey (ASAS; Pojmański 2002) and the Optical Monitoring Camera (OMC) on board the International Gamma-Ray Astrophysics Laboratory (INTEGRAL) satellite (Alfonso-Garzón et al. 2012). The light curves based on these data are shown in Fig. 3. The DASCH provides 1484 measurements of the *B* magnitude of Sk–69° 279 over the time interval of ≈1890–1985 with a gap between 1955 and 1970. After rejection of low quality data points, we are left with 553 measurements with a median value of 12.76±0.22 mag, which agrees with the mean *B* magnitude of 12.87±0.01, based on our CCD observations.

³ <https://archive.stsci.edu/>

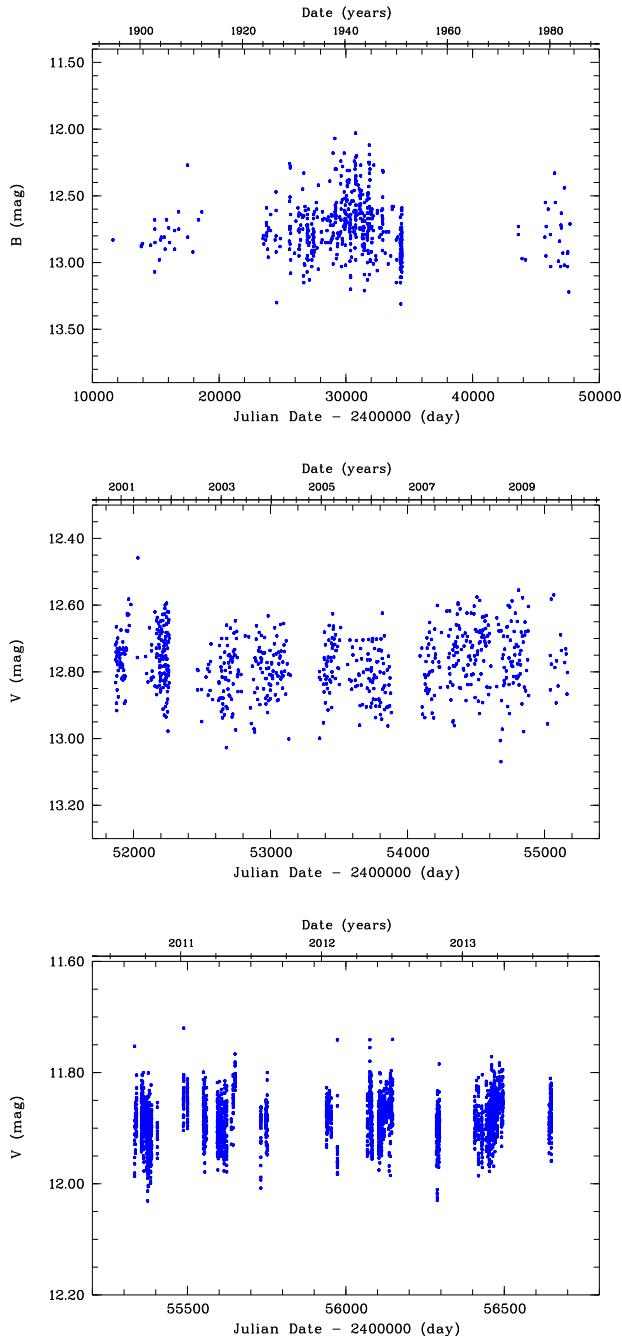


Figure 3. The Harvard DASCH (upper panel), ASAS (middle panel) and OMC-INTEGRAL (bottom panel) light curves of Sk-69° 279. Note that the bottom light curve systematically overestimates the brightness of Sk-69° 279 because of the large OMC photometric aperture (see the text for details).

Similarly, the ASAS light curve in the V -band (based on 733 measurements) shows that the brightness of the star in 2001–2009 varies by $\approx \pm 0.1$ mag around the median value of ≈ 12.8 mag. The OMC light curve of Sk-69° 279 (based on 2979 measurements) also shows that the V -band brightness varies by $\approx \pm 0.1$ mag. The OMC photometry, however, is contaminated by nearby stars within the 52.5×52.5 arc-

sec photometric aperture, which results in the systematic increase of the V magnitude by ≈ 0.9 mag.

4 SK-69° 279: SPECTRAL ANALYSIS AND STELLAR PARAMETERS

4.1 Classification of Sk-69° 279

Fig. 2 shows that the spectrum of Sk-69° 279 is dominated by emission lines of H, He I, He II, N II and C III, some of which show P Cygni profiles. Further emission lines in the spectrum (see Fig. 5) are permitted lines of O II, N III, C III, Si III-IV, and C IV.

To classify Sk-69° 279, we use the classification criteria of Conti & Alschuler (1971). Namely, the logarithm of the ratio of the EWs of the He I $\lambda 4471$ and He II $\lambda 4541$ lines (see Table 2), $\log(\text{EW}_{4471}/\text{EW}_{4541}) = 0.50 \pm 0.02$, indicates that Sk-69° 279 is an O9.5 star (see table 3 in Conti & Alschuler 1971). The more recent classification criteria of Sota et al. (2014; see their table 3) based on the ratios of peak intensities of absorption-line pairs, $I(\text{He II } \lambda 4541)/I(\text{He I } \lambda 4388) = 0.8$ and $I(\text{He II } \lambda 4200)/I(\text{He I } \lambda 4144) = 0.9$ (both slightly less than 1), and $I(\text{Si III } \lambda 4552)/I(\text{He II } \lambda 4541) \ll 1$, suggest that Sk-69° 279 is an O9.2 star. The same spectral type also follows from the classification scheme for O stars based on the ratio of EWs of the lines He I $\lambda 4922$ and He II $\lambda 5411$ (Kerton, Ballantyne & Martin 1999):

$$\text{SpT} = (9.04 \pm 0.10) + (4.10 \pm 0.23) \log(\text{EW}_{4922}/\text{EW}_{5411}).$$

Using this equation and EWs from Table 2, one finds $\text{SpT} = 9.26$.

To determine the luminosity class of Sk-69° 279, we use table 5 in Conti & Alschuler (1971) and EWs of the Si IV $\lambda 4089$ and He I $\lambda 4144$ lines from Table 2. With $\log(\text{EW}_{4089}/\text{EW}_{4144}) = 0.56 \pm 0.02$, one finds that Sk-69° 279 is a supergiant, which agrees with location of this star in the LMC (cf. Nandy et al. 1984). Similarly, using the dependence of EW of the Si IV $\lambda 4483$ emission line on the luminosity class of O stars (see fig. 4 in Morrell, Walborn & Fitzpatrick 1991) and the measured $\text{EW}_{4483} = 140 \text{ m}\text{\AA}$ (see Table 2), one finds that the luminosity class of Sk-69° 279 is either Ia or Iab, while the ratio $I(\text{Si IV } \lambda 4089)/I(\text{He I } \lambda 4026) < 1$ allows one to narrow down the luminosity class to Ia (see table 6 in Sota et al. 2011).

The presence of the He II $\lambda 4686$ and N III $\lambda \lambda 4634\text{--}40\text{--}42$ emission lines indicates that Sk-69° 279 is an Of star (e.g. Sota et al. 2011), we therefore add a suffix ‘f’ to the spectral subtype, which then becomes O9.2 Iaf.

Using $B - V = 0.06 \pm 0.01$ (see Section 3.2) and the intrinsic colour of late O supergiants of $(B - V)_0 = -0.26$ mag (Martins & Plez 2006), one finds the colour excess of $E(B - V) = 0.32 \pm 0.01$ mag towards Sk-69° 279, which is in a good agreement with independent estimates derived in Sections 4.2 and 5. With the distance modulus for the LMC of 18.49 and assuming $A_V = 3.1E(B - V)$ (cf. Howarth 1983), one obtains the absolute visual magnitude $M_V = -6.67 \pm 0.03$ mag. Then, with $T_{\text{eff}} = 24 \text{ kK}$ (see Table 4 in the next section) and $\text{BC} = -2.34 \pm 0.05$ mag (Crowther, Lennon & Walborn 2006), one finds $M_{\text{bol}} = -9.01 \pm 0.06$ mag and $\log(L_*/L_\odot) = 5.50 \pm 0.02$, which well agrees with the results of spectral modelling.

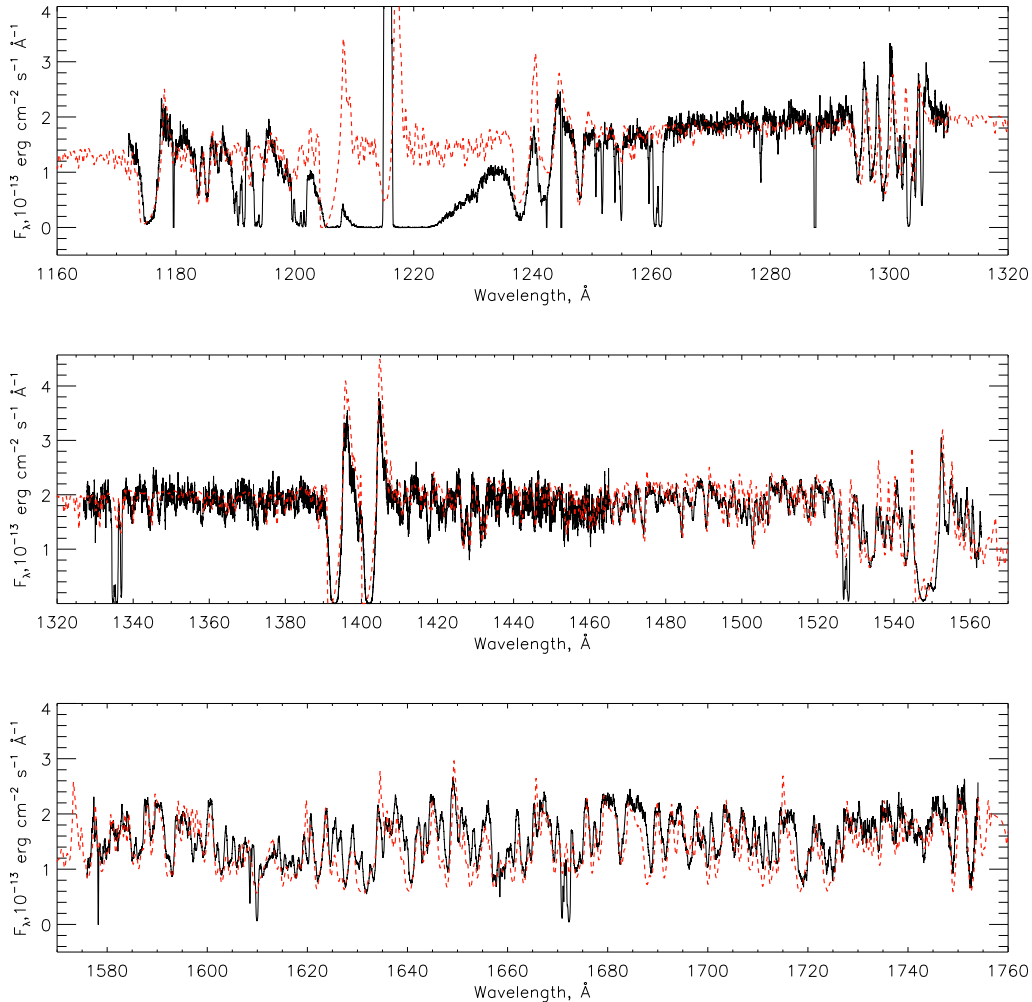


Figure 4. Comparison of the HST/COS UV spectrum (black solid line) with the model one (red dashed line), scaled to the distance to LMC and reddened by $E(B - V) = 0.31$ mag.

4.2 Spectral modelling

To determine the stellar parameters we have used the CMFGEN model atmosphere code (Hillier & Miller 1998). This code solves the radiative transfer equations for objects with spherically symmetric extended outflows using either the Sobolev approximation or the full comoving-frame solution of the radiative transfer equation. CMFGEN incorporates line blanketing, the effect of Auger ionization and clumping. Every model is defined by the hydrostatic stellar radius R_* , bolometric luminosity L_* , mass-loss rate \dot{M} , volume filling factor f , wind terminal velocity v_∞ , stellar mass M_* , and abundances of included chemical elements Z_i . Our calculations included H, He, C, N, O, Si, S, P and Fe. The mass-loss rate, density, and velocity are related to each other via the continuity equation. The best-fitting model is shown in Fig. 4 (UV range) and Fig. 5 (optical range)⁴.

As an initial photospheric density structure we adopted

the TLUSTY hydrostatic model atmosphere of Hubeny & Lanz (1995) and Lanz & Hubeny (2003) for deep quasi-static layers, which are connected to the wind with standard β -velocity law just above the sonic point. The β -velocity law is one of the basic simplifications typically adopted when constructing atmospheric models of hot stars. The radiation-driven wind theory (Puls et al. 1996; Lamers & Cassinelli 1999) predicts values of $\beta = 0.5 - 1$. Our study, however, suggests that a model with $\beta=3$ and the connection point located at approximately 40 km s^{-1} describes the observed spectrum better than models with other values of β and the connection point at 10 or 5 km s^{-1} . Although the values as high as $\beta = 3 - 3.5$ disagree with the theoretical predictions, they were often employed in modelling of (c)LBVs and blue supergiants (e.g., Kudritzki et al. 1999; Groh et al. 2009; Evans et al. 2004; Mahy et al. 2016). One of the first discussions of the discrepancy between the modelling results and the theoretical predictions is given in Hillier et al. (2003).

For measuring the stellar temperature T_* (determined at the radius where the Rosseland optical depth is 20) and the effective temperature T_{eff} (determined at the radius at

⁴ Note that the [N II] $\lambda\lambda 6548, 84$ lines visible in the HRS spectrum are of nebular origin (see Section 5).

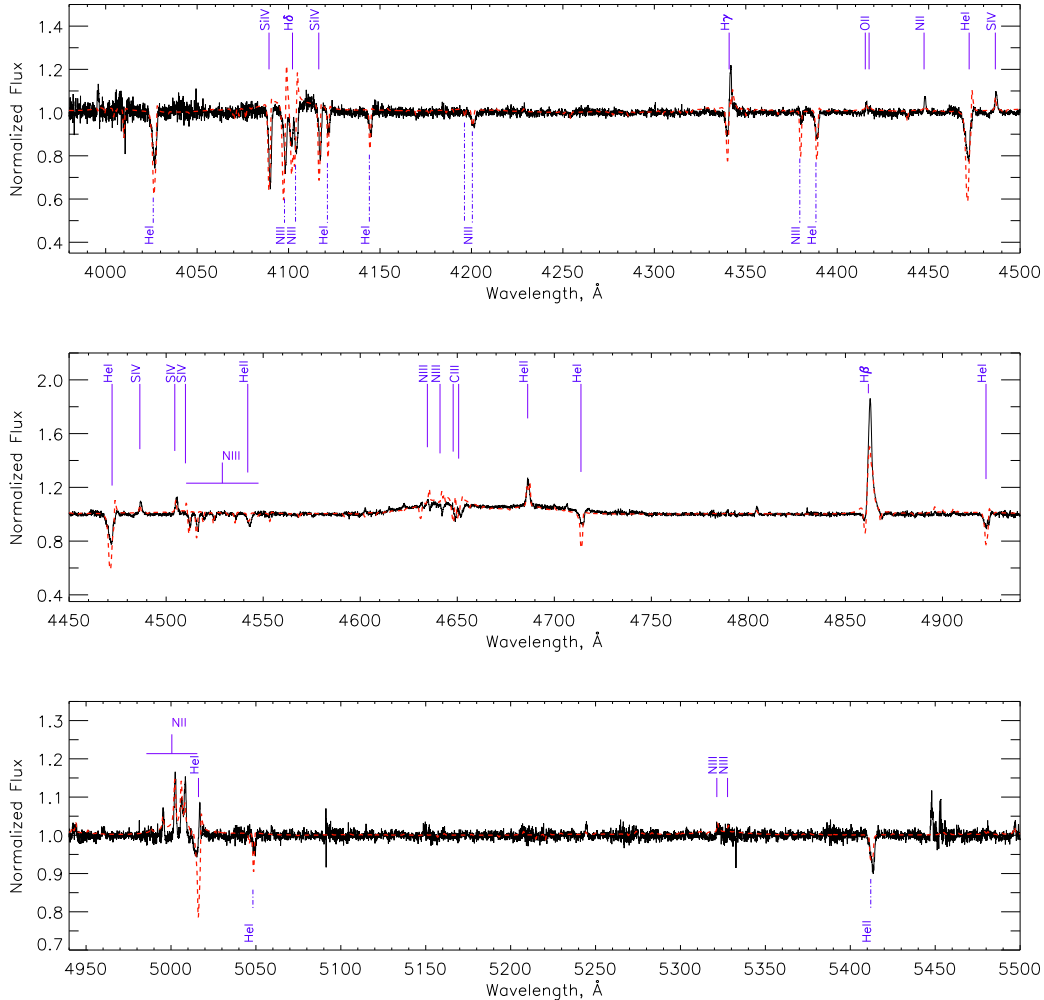


Figure 5. Normalized HRS spectrum of Sk-69° 279 taken on 2016 October 27 (black solid line), compared with the best-fitting CMFGEN model (red dashed line) with the parameters as given in Table 4.

which the Rosseland optical depth is $2/3$) with CMFGEN, we compared the intensities of different ion lines (He I, II; C III, IV; N II, III; Si III, IV) in the HRS spectrum, i.e., we used the traditional ionization-balance method.

To determine the luminosity of Sk-69° 279, we recomputed the fluxes for the distance to the LMC. The resulting fluxes were corrected for the interstellar extinction, and then compared to the calculated spectra convolved with the transmission curves of the standard B , V and I_c filters.

The colour excess $E(B - V)$ towards Sk-69° 279 was estimated by comparing the spectral energy distribution (SED) in the model spectrum with the observed UV and HRS spectra and photometric measurements compiled in Table 3. We found that the slopes of the model and observed spectra match each other if $E(B - V) = 0.31$ mag (Fig. 6). This value is within the error margins of $E(B - V) = 0.34 \pm 0.02$ mag derived from the Balmer decrement in the spectrum of the circumstellar shell (see Section 5).

As a next step, v_∞ and \dot{M} were estimated by using lines with P Cygni profiles and intensities of the emission lines. Our modelling also included the clumping described by the volume filling factor $f = \bar{\rho}/\rho(r)$, where $\bar{\rho}$ is the homogeneous

(unclumped) wind density and ρ is the density in clumps. It is assumed that the clumps are optically thin, while the interclump medium is void (Hillier & Miller 1999).

The filling factor depends on the radius as $f(r) = f_\infty + (1 - f_\infty) \exp(-v(r)/v_{cl})$, where f_∞ describes the density contrast and v_{cl} is a characteristic velocity at which clumping starts to be important. Šurlan et al. (2012, 2013) demonstrated that the clumping starts in the innermost layers of the wind, therefore we adopted $v_{cl} = 5 \text{ km s}^{-1}$ and determined $f_\infty = 0.5$ by fitting emission lines. Puls et al. (2006) and Najarro, Hanson & Puls (2011) studied the radial distribution of the clumping by simultaneous modelling of $H\alpha$, infrared, millimetre, and radio observations, and demonstrated that it decreases at large radii. And indeed, our computations show that, after adjusting all other parameters, the profiles of the $H\alpha$ and $H\beta$ lines are reproduced better if the clumping starts to disappear at velocities greater than 700 km s^{-1} .

The simultaneous presence of ‘hot’ (e.g. He II $\lambda\lambda 4686, 5411$) and ‘cold’ (e.g. N II $\lambda\lambda 6482, 6611$) lines in the spectrum suggests that Sk-69° 279 has an extended atmosphere with a large difference between T_* and T_{eff} . In Fig. 7, we

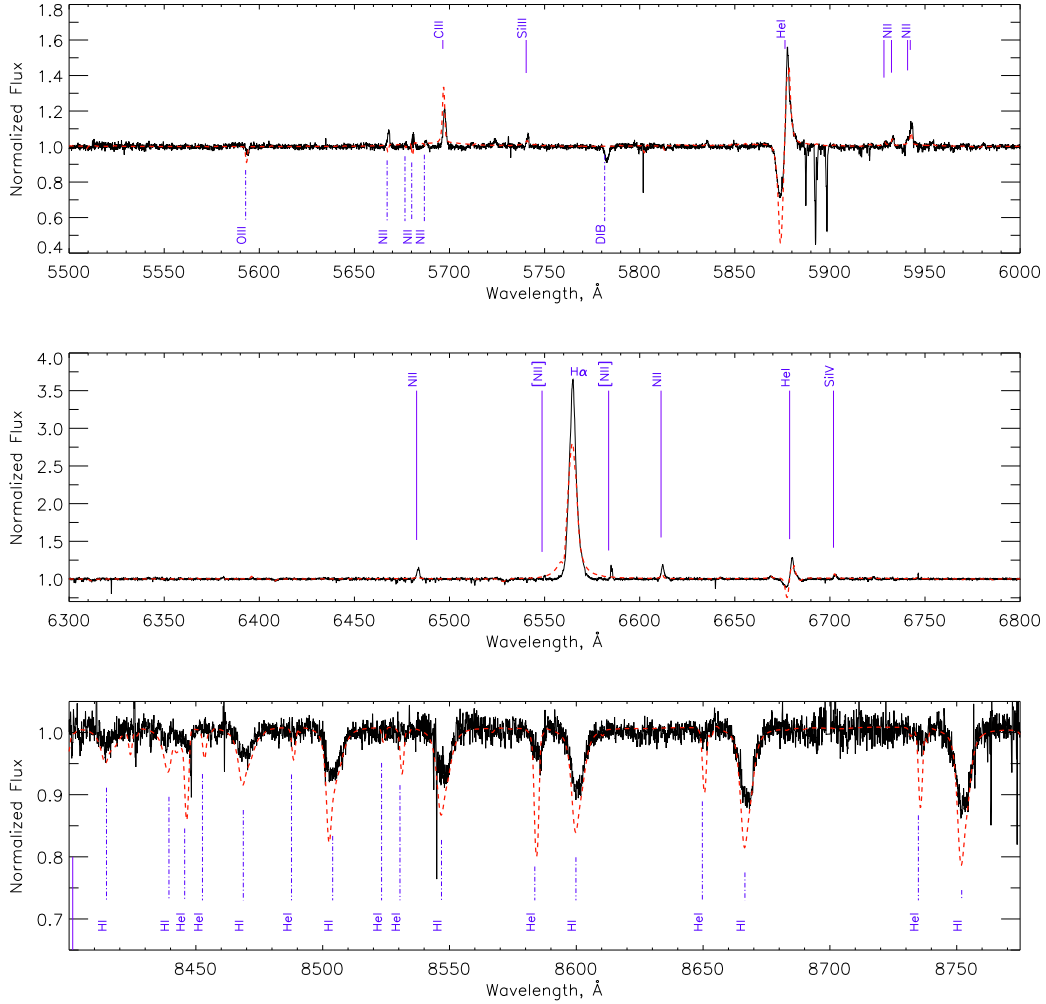


Figure 5. (Continued)

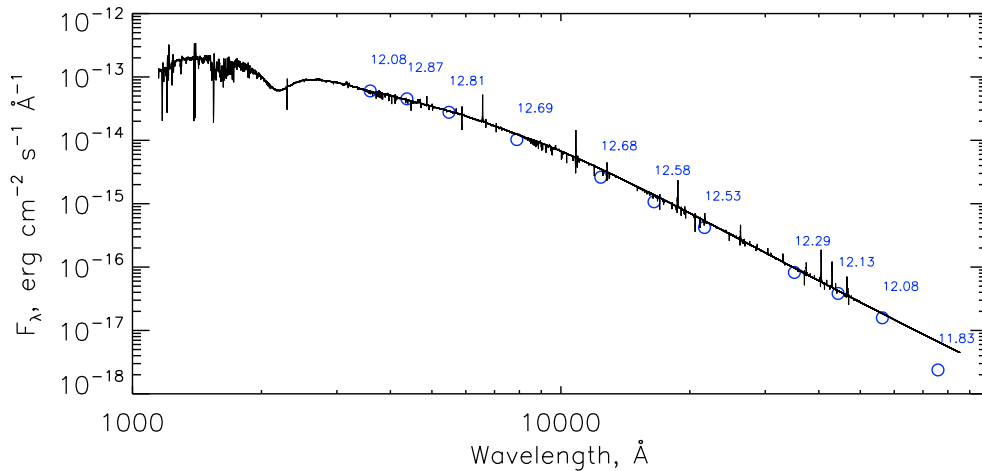


Figure 6. Observed flux distribution of Sk-69° 279 in absolute units, based on the photometric measurements (blue circles) compiled in Table 3, compared to the emergent flux of the reddened model spectrum (black/noisy line) with the parameters as given in Table 4.

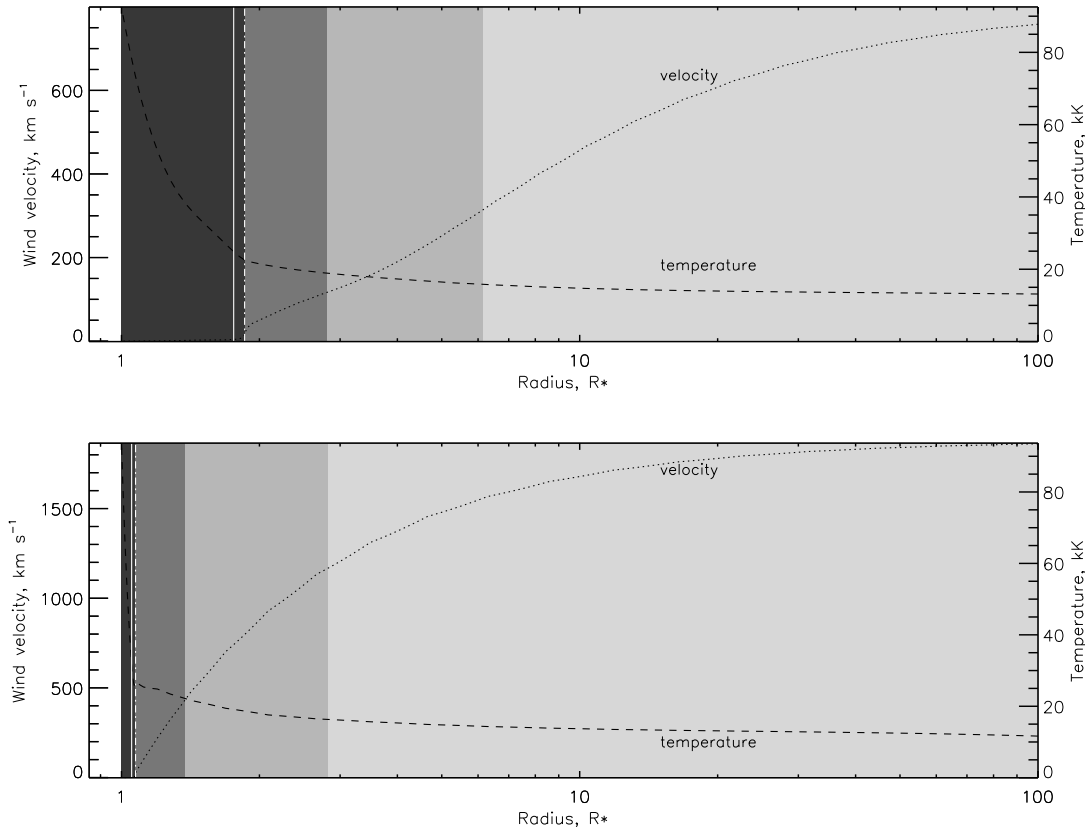


Figure 7. The wind structure of the best-fit CMFGEN model atmosphere of *Sk-69° 279* (upper panel) and a model atmosphere of an O9 supergiant (Martins et al. 2005). The differently coloured regions correspond, from left to right, to densities $n_e > 10^{12} \text{ cm}^{-3}$, $10^{12} > n_e > 10^{11} \text{ cm}^{-3}$, $10^{11} > n_e > 10^{10} \text{ cm}^{-3}$, $10^{10} > n_e > 10^9 \text{ cm}^{-3}$, and $n_e < 10^9$. The white vertical solid and dot dashed lines correspond, respectively, to a radius at which the Rosseland optical depth equals 2/3 and to a sonic radius. Black dotted and dashed lines plot, respectively, the wind velocity and temperature profiles as a function of radius (on a logarithmic scale).

plot the density, temperature and velocity profiles of our best-fit model atmosphere corresponding to $T_* \approx 30 \text{ kK}$ and $T_{\text{eff}} \approx 24 \text{ kK}$ (upper panel) and the model atmosphere of a ‘normal’ O9 supergiant (lower panel; Martins, Schaerer & Hillier 2005). Comparison of the panels shows that *Sk-69° 279* has a more inflated atmosphere and a much slower wind velocity as compared with blue supergiants of similar spectral type (e.g. Markova et al. 2003; Mokieim et al. 2007). This could be connected with the bi-stability jump mechanism (Pauldrach & Puls 1990; Lamers & Pauldrach 1991), which is manifested in a factor of 2 decrease in v_∞ when T_{eff} drops below a critical value of $\approx 21 - 25 \text{ kK}$ (Vink, de Koter & Lamers 1999), and in a drastic increase in \dot{M} (Lamers, Snow & Lindholm 1995; Vink et al. 1999), accompanied by the formation of an extended atmosphere (Smith, Vink & de Koter 2004).

With the 2016’s HRS spectrum, we also estimated the projected rotational and heliocentric radial velocities of *Sk-69° 279*. To determine the projected rotational velocity, $v \sin i$, we used the correlations between this velocity and FWHMs of the He I $\lambda\lambda 4026, 4144, 4388$ and 4471 lines; see equations (1)–(4) in Steele, Negueruela & Clark (1999). For $\text{FWHM}(4026) = 2.49 \pm 0.04 \text{ \AA}$, $\text{FWHM}(4144) = 1.57 \pm 0.06 \text{ \AA}$, $\text{FWHM}(4388) = 1.95 \pm 0.03 \text{ \AA}$ and $\text{FWHM}(4471) = 2.93 \pm 0.05 \text{ \AA}$, we found $v \sin i \approx 114, 70, 82$ and 121 km s^{-1} , respec-

tively, with a mean value of $97 \pm 10 \text{ km s}^{-1}$ (here we conservatively set the margins of error of 10 km s^{-1}). This figure should be considered as an upper limit to the projected rotational velocity because the lines might be broadened because of macroturbulence. Note that a similar value of $v \sin i$ of $84 \pm 10 \text{ km s}^{-1}$ was derived by Penny & Gies (2009) from UV lines in the *Far Ultraviolet Spectrographic Explorer (FUSE)* spectrum of *Sk-69° 279*.

The heliocentric radial velocity of *Sk-69° 279* was obtained using RVs of lines not affected by P Cygni absorptions. We found the mean value of RV of $226 \pm 3 \text{ km s}^{-1}$, which agrees with the systemic velocity of the shell (see Section 5). To search for possible radial velocity variability, we carried out a cross-correlation analysis on the two HRS spectra in the spectral range of $8460 - 8765 \text{ \AA}$, which is dominated by Paschen absorption lines. We found that in the second spectrum these lines become shifted bluewards by $16.3 \pm 0.2 \text{ km s}^{-1}$. Although this change in the radial velocity might be caused by the duplicity of the star, the more likely explanation is that it is due to the photospheric variability, which is typical of luminous blue supergiants. For example, similar radial velocity variations were detected in the spectra of two blue supergiants with bipolar circumstellar nebulae, *Sher 25* (Smartt et al. 2002; Taylor et al. 2014)

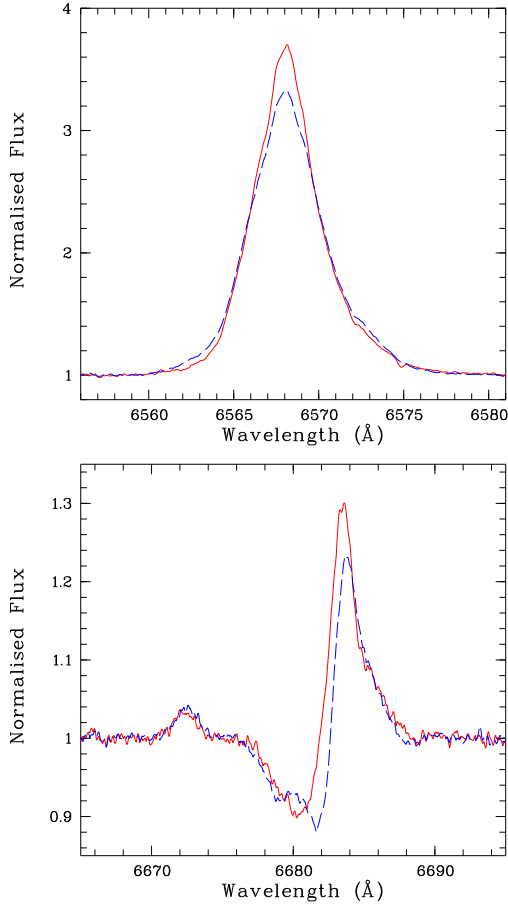


Figure 8. Changes in the H α (upper panel) and He I λ 6678 (bottom panel) line profiles: 2016 October 27 (red solid line) and 2017 September 26 (blue dashed line).

and HD 168625 (Mahy et al. 2016), both of which are considered to be cLBVs.

Comparison of the HRS spectra revealed further signatures of the wind variability. Namely, we found that i) the intensity of the H α and H β lines has decreased by about 10 per cent in 2017, while the RVs of these lines remain the same (Fig. 8), ii) the He II $\lambda\lambda$ 4541, 4686 and 5412 lines become shifter redwards, and iii) P Cygni profiles of He I lines (e.g. He I $\lambda\lambda$ 4471, 4921, 5015, 5876 and 6678) show changes in their red wings, while the blue ones remain intact (see Fig. 8).

A summary of the parameters of Sk-69° 279 derived above is given in Table 4. To this table we also added surface abundances of the basic elements in the atmosphere of Sk-69° 279 and their uncertainties.

The He/H abundance ratio was estimated by iterative adjustment of this ratio along with other physical parameters of the star to reproduce the overall shape of all He and H lines visible in both, UV and optical, spectra.

The nitrogen abundance was estimated by analysing the behaviour of all nitrogen lines in the optical range. As seen from Fig. 5, we obtained more or less good fits for the N III $\lambda\lambda$ 3999, 4004, N III $\lambda\lambda$ 4510-47, N II $\lambda\lambda$ 4987, 4994 and 5002-25 lines. On the other hand, one can see that in the model spectrum the N III $\lambda\lambda$ 4634-40 lines are in emission, while

Table 4. Stellar parameters for Sk-69° 279.

| | |
|---|------------------------------|
| $\log(L_*/L_\odot)$ | 5.54 ± 0.06 |
| $\log(\dot{M}/M_\odot \text{ yr}^{-1})$ | -5.26 ± 0.04 |
| R_* (R_\odot) | 22.7 ± 2.3 |
| T_* (kK) | 29.5 ± 0.5 |
| $R_{2/3}$ (R_\odot) | 35.5 ± 5.5 |
| T_{eff} (kK) | $24.0^{+0.5}_{-1.5}$ |
| v_∞ (km s^{-1}) | 800 ± 100 |
| f_∞ | 0.5 |
| β | 3.0 (fixed) |
| $v \sin i$ (km s^{-1}) | 97 ± 10 |
| $E(B-V)$ (mag) | 0.31 (fixed) |
| M_{bol} (mag) | -9.11 ± 0.15 |
| M_V (mag) | -6.70 ± 0.15 |
| He (mass fraction) | 0.50 \pm 0.07 |
| C (mass fraction) | $2.3 \pm 1.5 \times 10^{-4}$ |
| N (mass fraction) | $2.8 \pm 0.8 \times 10^{-3}$ |
| O (mass fraction) | $1.2 \pm 0.4 \times 10^{-3}$ |
| Si (mass fraction) | $2.4 \pm 0.4 \times 10^{-4}$ |
| S (mass fraction) | $1.0 \pm 0.2 \times 10^{-4}$ |

in the observed one they are in absorption. There is also a discrepancy in fitting the N II $\lambda\lambda$ 5666-86 lines. These discrepancies may probably be overcome by using a more complicated velocity law for lower parts of the wind where the former lines are forming, and by constructing a more expanded atmosphere, because the latter lines appear in emission when the temperature decreases to 23 kK.

The O II $\lambda\lambda$ 4415, 4417 and O III λ 5592 lines were used to estimate the oxygen abundance, while the C IV $\lambda\lambda$ 5801, 5812 and C III $\lambda\lambda$ 1175, 1247 lines – to derive the abundance of carbon. We did not use other carbon lines, e.g. C III $\lambda\lambda$ 4647, 4650, 4652 and C III λ 5696, to derive the abundance of this element because they are sensitive to a variation of T_{eff} , \dot{M} and the surface gravity $\log g$, and to the inclusion of other ions, e.g., Fe IV, Fe IV and Si IV, in calculations (Martins & Hillier 2012). We also determined the abundances of silicon and sulphur using lines of these elements detected in the HRS spectrum. For the abundances of phosphorus and iron-group elements we adopted half-solar values because of the low metallicity of the LMC ($Z = Z_\odot/2$).

5 SPECTROSCOPIC OBSERVATIONS OF THE CIRCULAR SHELL

As noted in Section 3.1, the RSS spectrum of the nebula was obtained with the slit oriented south-north ($\text{PA}=0^\circ$) and placed on the star. In the two-dimensional (2D) spectrum of the shell we detected the emission lines of H γ , H β , H α , He I λ 5876, [N II] $\lambda\lambda$ 6548, 6584 and [S II] $\lambda\lambda$ 6717, 6731. All of them are visible on both sides of Sk-69° 279. The [O III] $\lambda\lambda$ 4959, 5007 lines are absent, which indicates a low ionization state in the shell.

The upper panel in Fig. 9 plots the H α and [N II] λ 6584 emission line intensities along the slit. Both lines appear everywhere along the slit and their peak intensities show clear correlation with the shell. In the northern direction the slit crosses a region of enhanced brightness (identified as knot N in Weiss et al. 1997), which is manifested in a factor of two higher intensity of the lines. This panel also shows that

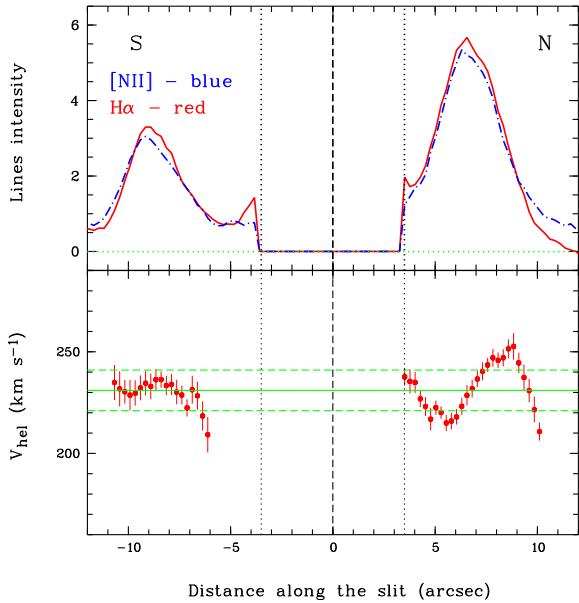


Figure 9. Upper panel: Variation along the slit of the $H\alpha$ and $[N\text{II}]\ \lambda 6584$ emission line intensities in the spectrum of the circular shell, shown, respectively, with a solid (red) and dashed (blue) lines. Bottom panel: $H\alpha$ heliocentric radial velocity distribution along the slit. The (green) solid and dashed horizontal lines show, respectively, the systemic velocity of the shell of $\approx 230\text{ km s}^{-1}$ and its error margins. The dashed vertical line in both panels corresponds to the position of *Sk-69° 279*, while the dotted vertical lines at ± 3.5 arcsec from the central line mark the area where the emission line intensities and the $H\alpha$ radial velocity were not measured because of the effect of the star. S–N direction of the slit is shown.

the star is offset by ≈ 1 arcsec towards the brighter part of the shell. The offset and the brightness asymmetry might be caused by either interstellar medium density gradient in the north-south direction (cf. Section 2) or by stellar motion to the north (cf. Section 6), or by both effects. The bottom panel in Fig. 9 shows the distribution of the $H\alpha$ heliocentric radial velocity along the slit. Using this distribution, we estimated the systemic heliocentric radial velocity of the shell to be $\approx 230 \pm 10\text{ km s}^{-1}$, which agrees with that measured by Weis et al. (1997), and is offset by 20 km s^{-1} with respect to the background H II region.

The nebular forbidden lines of $[N\text{II}]$ are also visible in the HRS spectra of *Sk-69° 279*, where they are resolved in two components (see Fig. 10), originating in the approaching and receding sides of the circumstellar shell. The heliocentric radial velocities of these components are, respectively, 215.3 ± 0.5 and $243.7 \pm 0.6\text{ km s}^{-1}$, implying the systemic velocity of the shell of $\approx 230\text{ km s}^{-1}$, which is in a good agreement with the estimate based on the RSS spectrum.

1D RSS spectra of the shell were extracted from a region of radius of 10 arcsec centred on *Sk-69° 279* with the central ± 3.5 arcsec excluded. The resulting spectrum is presented in Fig. 11. Table 5 gives the observed intensities of all detected lines normalized to $H\beta$, $F(\lambda)/F(H\beta)$, as well as the reddening-corrected line intensity ratios, $I(\lambda)/I(H\beta)$, and the logarithmic extinction coefficient, $C(H\beta)$. The latter corresponds to the colour excess of $E(B-V) = 0.34 \pm 0.02$

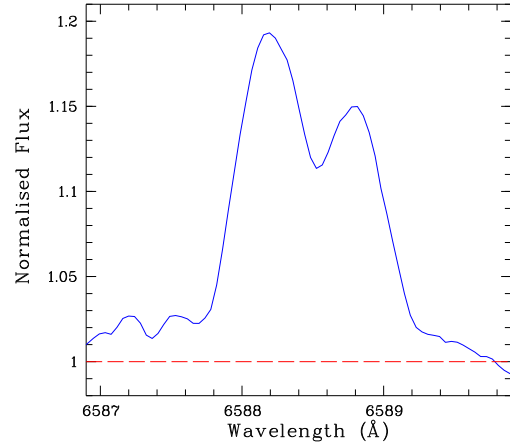


Figure 10. Double-peak profile of the $[N\text{II}]\ \lambda 6584$ line.

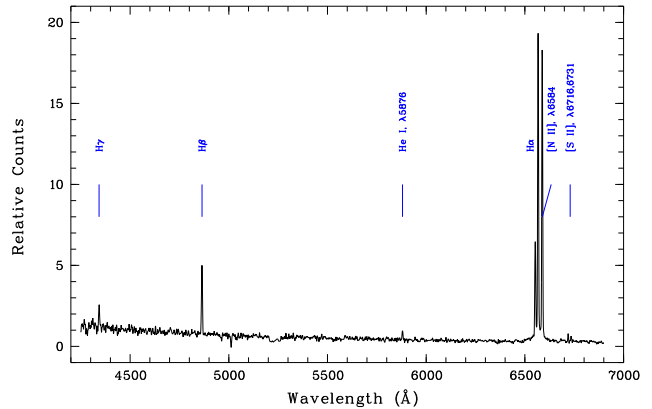


Figure 11. 1D reduced spectrum of the circular shell obtained with the SALT. All detected emission lines are marked.

mag. The lines in Table 5 were measured with program described in Kniazev et al. (2004). We also derived the electron number density using the the $[S\text{II}]\ \lambda\lambda 6716, 6731$ lines, $n_e([S\text{II}])$ and added then to Table 5. The obtained density is at the low end of the range of densities measured for circumstellar nebulae around LBVs (Nota et al. 1995; Smith et al. 1998), which is understandable given the large extent of the shell (cf. Weis et al. 1997). To calculate $C(H\beta)$ and $n_e([S\text{II}])$, we assumed that $T_e = 10^4\text{ K}$; for lower values of T_e the derived figures remain almost the same.

Using the reddening-corrected intensities of the $[N\text{II}]$ and $[S\text{II}]$ lines, we estimated the nitrogen to sulphur abundance ratio, which, according to Benvenuti, D’Odorico & Peimbert (1973; and references therein) is given by:

$$\frac{N(N^+)}{N(S^+)} = 3.61 \frac{I(6584)}{I(6716 + 6731)}.$$

This ratio is almost independent of n_e and T_e , provided that these parameters are, respectively, $\leq 1000\text{ cm}^{-3}$ and $\leq 10^4\text{ K}$. Although our spectrum of the shell did not allow us to estimate T_e , it is reasonable to assume that it is $\leq 10^4\text{ K}$ (see, e.g., Nota et al. 1995; Smith et al. 1998). Using the above equation and Table 5, one finds $N(N^+)/N(S^+) \approx 94.7_{-13.1}^{+16.7}$, where the error margins were derived from the uncertainties on the line intensities. Similarly, we estimated

Table 5. Line intensities of the circular shell around Sk–69 279.

| $\lambda_0(\text{\AA})$ Ion | F(λ)/F(H β) | I(λ)/I(H β) |
|-----------------------------|-------------------------------------|------------------------------|
| 4340 H γ | 0.367 \pm 0.028 | 0.427 \pm 0.033 |
| 4861 H β | 1.000 \pm 0.038 | 1.000 \pm 0.038 |
| 5876 He I | 0.134 \pm 0.013 | 0.105 \pm 0.010 |
| 6548 [N II] | 1.333 \pm 0.037 | 0.912 \pm 0.028 |
| 6563 H α | 4.305 \pm 0.126 | 2.937 \pm 0.094 |
| 6584 [N II] | 4.013 \pm 0.109 | 2.727 \pm 0.082 |
| 6717 [S II] | 0.089 \pm 0.010 | 0.059 \pm 0.007 |
| 6731 [S II] | 0.068 \pm 0.009 | 0.045 \pm 0.006 |
| C(H β) | 0.50 \pm 0.04 | |
| $E(B - V)$ | 0.34 \pm 0.02 mag | |
| $n_e([\text{Si II}])$ | 94.0 $^{+289.0}_{-84.0}$ cm $^{-3}$ | |
| v_{hel} | 230 \pm 10 km s $^{-1}$ | |

the $N(N^+)/N(S^+)$ ratio in the surrounding H II region to be 1.42 ± 0.14 , which agrees within the margins of error with the value of $2.75_{-1.17}^{+2.04}$ measured for H II regions in the LMC (Russell & Dopita 1992). Since the S abundance do not change much in the course of stellar evolution, one can conclude that the N abundance in the shell is elevated by a factor of $\approx 34_{-17}^{+36}$ with respect to the LMC value, and that the shell is composed mostly of the CNO-processed wind/ejecta material from Sk–69° 279 (cf. Weis et al. 1997). This conclusion is supported by the estimate of the surface N abundance of Sk–69° 279 (see Table 4), which is enhanced by about the same factor as in the shell (see next section). Using the LMC abundances of N and S from Russell & Dopita (1992), we derive a N abundance of the shell of $\log(N/H) + 12 = 8.68$. We caution that this value could be somewhat overestimated if the shell contains some amount of S^{++} .

6 DISCUSSION

From Table 4 it follows that the surface of Sk–69° 279 is highly enriched with nitrogen, while the total surface C+N+O abundance agrees within the error margins with the LMC metallicity, implying that there is CNO-processed material on the stellar surface. Fig. 12 shows the position of Sk–69° 279 in the Hertzsprung-Russell diagram along with evolutionary tracks from Brott et al. (2011) for (single) stars with the LMC metallicity and two values of the initial rotational velocity, v_{init} , of ≈ 100 and 400 km s $^{-1}$. If Sk–69° 279 was originally born as a single star, then one can infer that its initial mass was $M_{\text{init}} \approx 30 - 35 M_{\odot}$ and that this star is either near the end of the main sequence phase or has recently left it. The enhanced N abundances in atmospheres of main sequence O and early-B stars was discovered by Lyubimkov (1984) and interpreted as an indicator of deep internal mixing of the CNO cycle products. Since the beginning of 2000's the mixing is included in stellar evolution models (e.g. Heger & Langer 2000; Meynet & Maeder 2000) and it is believed that it is caused by the stellar rotation. Whether the rotational mixing is the main cause of enhanced surface N abundance in some OB stars is, however, still a subject of debate. Besides the fast stellar rotation, the surface N abundance could also be enhanced because of binary interaction processes (e.g. Langer 2012; see also below).

The models by Brott et al. (2011) show that the higher v_{init} and M_{init} of a star the higher its surface He and N abundances. For stars with $M_{\text{init}} \approx 30 - 35 M_{\odot}$ and $v_{\text{init}} \gtrsim 400$ km s $^{-1}$ the rotationally induced mixing can enhance these abundances, respectively, by factors of $\sim 2 - 3$ and 30 well before the stellar surface will become enriched by fusion products because of the first dredge-up.

In Table 6, we compare Sk–69° 279 with three model stars from Brott et al. (2011) with the following initial masses and rotational velocities: $M_{\text{init}} = 30 M_{\odot}$, $v_{\text{init}} = 407$ km s $^{-1}$ (hereafter model 1), $M_{\text{init}} = 30 M_{\odot}$, $v_{\text{init}} = 439$ km s $^{-1}$ (model 2), and $M_{\text{init}} = 35 M_{\odot}$, $v_{\text{init}} = 362$ km s $^{-1}$ (model 3). The last row of the table gives factors by which the N abundances of Sk–69° 279 and the model stars are enhanced with respect to the LMC N abundance of 1.0×10^{-4} (a value adopted in Brott et al. 2011). One can see that all three models reproduce fairly good the main parameters of Sk–69° 279, such as T_{eff} , L_* and the surface abundances, and suggest that this star is $\approx 6 - 6.5$ Myr old. In models 1 and 3, the predicted \dot{M} and the He and N abundances are somewhat lower than the values derived for Sk–69° 279. These quantities, however, increase with the increase of v_{init} and in model 2 they better match the corresponding parameters of Sk–69° 279 (the C and O abundances predicted by this model, however, are lower than in Sk–69° 279). Interestingly, when the star transitions from core-H to core-He burning and contracts, model 2 shows a factor of 10 increase in \dot{M} on a time scale of ~ 1000 yr 5 , while other stellar parameters remain almost intact and comparable to those of Sk–69° 279, except of the surface rotational velocity, v_{surf} , which slows down by ≈ 30 per cent on the same time scale. For even higher v_{init} , the mass fractions of He and N on the surface of a $30 M_{\odot}$ star increase, respectively, to ≈ 0.8 and 3×10^{-3} . Such fast-spinning stars, however, are much hotter than Sk–69° 279 and remain always in the blue part of the Hertzsprung-Russell diagram.

Table 6 also shows that v_{surf} of all three model stars is higher than $v \sin i$ measured for Sk–69° 279. Although we cannot exclude the possibility that Sk–69° 279 is oriented nearly pole-on and therefore its rotational velocity is actually higher, it is also possible that this (presumably initially fast-spinning) star has reached the limit of hydrostatic stability (Ω -limit; Langer 1997, 1998) and ejected its outer layers either instantly or during a brief episode of enhanced mass loss. If so, this might be responsible for the formation of the circumstellar shell and slowing down the stellar surface and its enrichment in helium and nitrogen. The origin of the shell around Sk–69° 279 could also be due to enhanced mass loss caused by the bi-stability jump, while the presumably high initial rotational velocity of this star may be significantly reduced because of the bi-stability braking (Vink et al. 2010).

While the major parameters of Sk–69° 279 could be explained fairly well in the framework of rapidly rotating single star models, it is also possible that this star is the product of binary evolution and that its enhanced He and N abundances are because of accretion of CNO-processed material

⁵ This increase in \dot{M} is related to the bi-stability jump (Vink, de Koter & Lamers 2000) and spinning up of the surface layers caused by the overall contraction of the star.

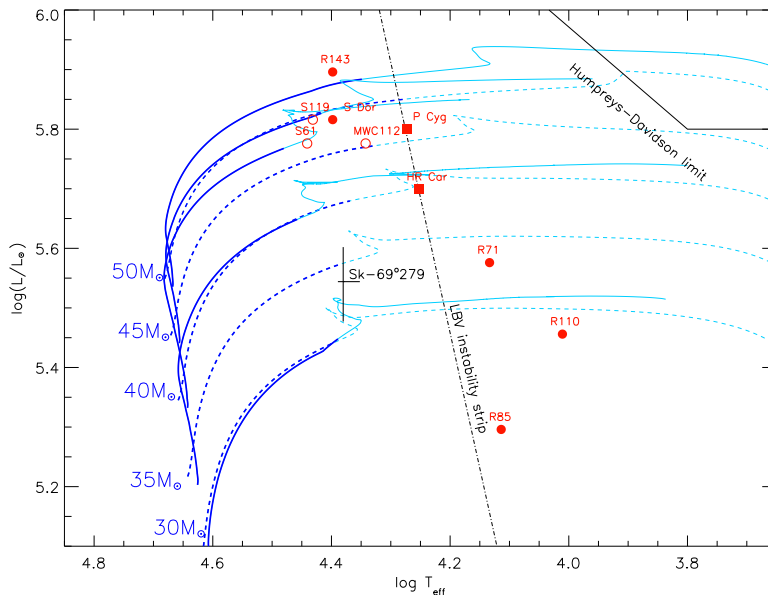


Figure 12. Position of *Sk-69° 279* in the Hertzsprung-Russell diagram. The LBV minimum instability strip is indicated by a dot dashed line (as defined in Groh et al. 2009) and the Humphreys-Davidson limit is shown with a solid (black) line. Positions of two Galactic bona fide LBVs P Cygni and HR Car (during its visual minimum) are shown with squares; their parameters are, respectively, from Najarro (2001) and Groh et al. (2009). Positions of bona fide and candidate LBVs in the LMC (Humphreys et al. 2016) are shown, respectively, with filled and open circles. The evolutionary tracks for rotating main sequence stars at the LMC metallicity are from Brott et al. (2011). The dashed and solid lines correspond, respectively, to initial rotational velocities of ≈ 110 and 400 km s^{-1} . The thick (blue) parts of the tracks correspond to the stage when a star burns the hydrogen in its core.

Table 6. Comparison of *Sk-69° 279* with three model stars from Brott et al. (2011). See the text for details.

| | <i>Sk-69° 279</i> | model 1 | model 2 | model 3 |
|---|-------------------|---------|---------|---------|
| $M_{\text{init}} (M_{\odot})$ | – | 30 | 30 | 35 |
| $v_{\text{init}} (\text{km s}^{-1})$ | – | 407 | 439 | 362 |
| age (Myr) | – | 5.9 | 6.5 | 5.9 |
| $T_{\text{eff}} (\text{kK})$ | 22.5–24.5 | 22.5 | 23.0 | 22.7 |
| $\log(L_*/L_{\odot})$ | 5.48–5.60 | 5.50 | 5.57 | 5.58 |
| $R_{2/3} (R_{\odot})$ | 30–41 | 37 | 38 | 40 |
| $\log(\dot{M}/M_{\odot} \text{ yr}^{-1})$ | -5.26 ± 0.04 | -5.47 | -5.22 | -5.43 |
| $v_{\text{surf}} (\text{km s}^{-1})$ | – | 233 | 521 | 191 |
| He (mass fraction) | 0.5 | 0.3 | 0.4 | 0.3 |
| C (mass fraction) (10^{-4}) | 0.8–3.8 | 1.3 | 0.5 | 1.7 |
| N (mass fraction) (10^{-3}) | 2.0–3.6 | 1.8 | 2.7 | 1.5 |
| O (mass fraction) (10^{-3}) | 0.8–1.6 | 1.1 | 0.3 | 1.3 |
| ΔN | 20–35 | 18 | 27 | 15 |

from the binary companion star or due to merger with this star. Both these processes could also be responsible for spinning up and rotational mixing of *Sk-69° 279*, and thereby for enhanced mass-loss and additional enrichment of the stellar surface in He and N. According to Sana et al. (2012, 2013), the majority of massive stars are members of binary systems and the evolution of many of them is strongly affected by interaction with a companion star already during the main sequence stage (see also de Mink et al. 2014).

The above considerations support the proposal by Lamers et al. (2001) that fast-rotating stars could produce LBV-like nebulae while they are at or near the end of the main sequence phase. The same conclusion was also

drawn from studies of the blue supergiants Sher 25 (B1.5 Iab; Smartt et al. 2002; Hendry et al. 2008), TYC 3159-6-1 (O9.5–O9.7 Ib; Gvaramadze et al. 2014a), [GKF2010] MN18 (B1 Ia; Gvaramadze et al. 2015) and HD 168625 (B6 Iap; Mahy et al. 2016), all of which are associated with compact circumstellar nebulae. The bipolar morphology of these nebulae strongly suggest that their central stars were nearly critical rotators in the past (the projected rotational velocities of these stars are similar to that of *Sk-69° 279*), while the CNO abundances of the stars indicate that they are either near the end of the main sequence or just evolved off it.

The ejection of the outer layers of fast-spinning stars

can not only result in the origin of circumstellar nebulae and slowing down these stars but, presumably, may also be accompanied by the LBV-like variability. The bloated atmosphere of Sk−69°279 and its moderate wind velocity may, therefore, be residual of the LBV activity in the recent past.

To conclude, we note that the 20 km s^{-1} difference between the radial velocities of the circumstellar shell and the local ISM hints at the possibility that Sk−69°279 is a runaway star (cf. Danforth & Chu 2001). This possibility is supported by the isolated location of this star from known star clusters (cf. Gvaramadze et al. 2012b). If the brightness asymmetry of the circumstellar shell around Sk−69°279 is caused by motion of this star to the north, then its possible birth place is the open star cluster [M87] OB 6 (Melnick 1987), located at about 5 arcmin (or ≈ 70 pc in projection) to the south. The age of this cluster of 15_{-10}^{+15} Myr (Glatt, Grebel & Koch 2010) agrees within the margins of error with the age of Sk−69°279 of ≈ 6 –6.5 Myr.

7 ACKNOWLEDGEMENTS

This work is based on observations obtained with the Southern African Large Telescope (SALT), programmes 2011-3-RSA_OTH-002, 2016-1-SCI-012 and 2017-1-SCI-006, and supported by the Russian Foundation for Basic Research grant 16-02-00148. AYK and OVM acknowledge support from, respectively, the National Research Foundation (NRF) of South Africa and the project RVO:67985815 in the Czech Republic. We are grateful to F. Martins for providing us the CMFGEN model of an O9I star. Some of the data presented in this paper were obtained from the Mikulski Archive for Space Telescopes (MAST), the Digital Access to a Sky Century @ Harvard (DASCH), and the OMC Archive at CAB (INTA-CSIC), pre-processed by ISDC. STScI is operated by the Association of Universities for Research in Astronomy, Inc., under NASA contract NAS5-26555. Support for MAST for non-HST data is provided by the NASA Office of Space Science via grant NNX09AF08G and by other grants and contracts. The DASCH project at Harvard is grateful for partial support from NSF grants AST-0407380, AST-0909073, and AST-1313370. This work has made use of the NASA/IPAC Infrared Science Archive, which is operated by the Jet Propulsion Laboratory, California Institute of Technology, under contract with the National Aeronautics and Space Administration, the SIMBAD data base and the VizieR catalogue access tool, both operated at CDS, Strasbourg, France.

REFERENCES

- Alfonso-Garzon J., Domingo A., Mas-Hesse J. M., 2010, Proc. Sci., First catalogue of variable sources observed by OMC onboard INTEGRAL. SISSA, Trieste, PoS(INTEGRAL 2010)069
- Barnes S. I. et al., 2008, in McLean I. S., Casali M. M., eds, Proc. SPIE Conf. Ser. Vol. 7014, Ground-based and Airborne Instrumentation for Astronomy II. SPIE, Bellingham, p. 70140K
- Benvenuti P., D’Odorico S., Peimbert M., 1973, A&A, 28, 447
- Berdnikov L., Vozyakova O. V., Kniazev A. Yu., Kravtsov V. V., Dambis A. K., Zhuiko S. V., 2012, Astron. Rep., 56, 290
- Bohannon B., 1997, in Nota A., Lamers H. J. G. L. M., eds, ASP Conf. Ser. Vol. 120, Luminous Blue Variables: Massive Stars in Transition. Astron. Soc. Pac., San Francisco, p. 120
- Bohannon B., Epps H. W., 1974, A&AS, 18, 47
- Bonanos A. Z. et al., 2009, AJ, 138, 1003
- Bramall D. G. et al., 2010, in McLean I. S., Ramsay S. K., Takami H., eds, Proc. SPIE Conf. Ser. Vol. 7735, Ground-based and Airborne Instrumentation for Astronomy III. SPIE, Bellingham, p. 77354F
- Bramall D. G. et al., 2012, in McLean I. S., Ramsay S. K., Takami H., eds, Proc. SPIE Conf. Ser. Vol. 8446, Ground-based and Airborne Instrumentation for Astronomy IV. SPIE, Bellingham, p. 84460A
- Brott I. et al., 2011, A&A, 530, A115
- Buckley D. A. H., Swart G. P., Meiring J. G., 2006, in Stepp L. M., ed., Proc. SPIE Conf. Ser. Vol. 6267, Ground-based and Airborne Telescopes. SPIE, Bellingham, p. 62670Z
- Burgh E. B., Nordsieck K. H., Kobulnicky H. A., Williams T. B., O’Donoghue D., Smith M. P., Percival J. W., 2003, in Iye M., Moorwood A. F. M., eds, Proc. SPIE Conf. Ser. Vol. 4841, Instrument Design and Performance for Optical/Infrared Ground-based Telescopes. SPIE, Bellingham, p. 1463
- Clark J. S., Larionov V. M., Arkharov A., 2005, A&A, 435, 239
- Clark J. S., Egan M. P., Crowther P. A., Mizuno D. R., Larionov V. M., Arkharov A., 2003, A&A, 412, 185
- Conti P. S., Alschuler W. R., 1971, ApJ, 170, 325
- Conti P. S., Garmany C. D., Massey P., 1986, AJ, 92, 48
- Crause L. A. et al., 2014, in Ramsay S. K., McLean I. S., Takami H., eds, Proc. SPIE Conf. Ser. Vol. 9147, Ground-based and Airborne Instrumentation for Astronomy V. SPIE, Bellingham, p. 91476T
- Crawford S. M. et al., 2010, in Silva D. R., Peck A. B., Soifer B. T., eds, Proc. SPIE Conf. Ser. Vol. 7737, Observatory Operations: Strategies, Processes, and Systems III. SPIE, Bellingham, p. 773725
- Crowther P. A., Lennon D. J., Walborn N. R., 2006, A&A, 446, 279
- Cutri R. M. et al., 2003, VizieR Online Data Catalog, 2246, 0
- Danforth C. W., Chu Y.-H., 2001, ApJ, 552, L155
- de Mink S. E., Sana H., Langer N., Izzard R. G., Schneider F. R. N., 2014, ApJ, 782, 7
- Evans C. J., Lennon D. J., Walborn N. R., Trundle C., Rix S. A., 2004, PASP, 116, 909
- Fazio G. G. et al., 2004, ApJS, 154, 10
- Gibson B. K., 2000, Mem. Soc. Astron. Ital., 71, 693
- Glatt K., Grebel E. K., Koch A., 2010, A&A, 517, A50
- Grindlay J., Tang S., Simcoe R., Laycock S., Los E., Mink D., Doane A., Champine G., 2009, in Osborn W., Robbins L., eds, ASP Conf. Ser. Vol. 410, Preserving Astronomy’s Photographic Legacy: Current State and the Future of North American Astronomical Plates. Astron. Soc. Pac., San Francisco, p. 101
- Groh J. H., Hillier D. J., Daminieli A., Whitelock P. A., Marang F., Rossi C., 2009, ApJ, 698, 1698
- Groh J. H. et al., 2009, ApJ, 705, L25
- Gvaramadze V. V., Kniazev A. Y., 2017, in Miroshnichenko A. S., Zharikov S. V., Korcakova D., Wolf M., eds., ASP Conf. Ser. Vol. 508, The B[e] Phenomenon. Forty Years of Studies. Astron. Soc. Pac., San Francisco, p. 207
- Gvaramadze V. V., Kniazev A. Y., Fabrika S., 2010, MNRAS, 405, 1047
- Gvaramadze V. V., Kroupa P., Pflamm-Altenburg J., 2010, A&A, 519, A33
- Gvaramadze V. V., Pflamm-Altenburg J., Kroupa P., 2011, A&A, 525, A17
- Gvaramadze V. V., Weidner C., Kroupa P., Pflamm-Altenburg J., 2012b, MNRAS, 424, 3037

- Gvaramadze V. V., Miroshnichenko A. S., Castro N., Langer N., Zharikov S. V., 2014a, *MNRAS*, 437, 2761
- Gvaramadze V. V. et al., 2012a, *MNRAS*, 421, 3325
- Gvaramadze V. V. et al., 2014b, *MNRAS*, 442, 929
- Gvaramadze V. V. et al., 2015, *MNRAS*, 454, 219
- Heger A., Langer N., 2000, *ApJ*, 544, 1016
- Hendry M. A., Smartt S. J., Skillman E. D., Evans C. J., Trundle C., Lennon D. J., Crowther P. A., Hunter I., 2008, *MNRAS*, 388, 1127
- Hillier D. J., Miller D. L., 1998, *ApJ*, 496, 407
- Hillier D. J., Miller D. L., 1999, *ApJ*, 519, 354
- Hillier D. J., Lanz T., Heap S. R., Hubeny I., Smith L. J., Evans C. J., Lennon D. J., Bouret J.-C., 2003, *ApJ*, 588, 1039
- Howarth I. D., 1983, *MNRAS*, 203, 301
- Hubeny I., Lanz T., 1995, *ApJ*, 439, 875
- Humphreys R. M., Weis K., Davidson K., Gordon M. S., 2016, *ApJ*, 825, 64
- Isserstedt J., 1975, *A&AS*, 19, 259
- Kerton C. R., Ballantyne D. R., Martin P. G., 1999, *AJ*, 117, 2485
- Kniazev A. Y., Gvaramadze V. V., 2015, in *Proceedings of the SALT Science Conference 2015 (SSC2015)*. Stellenbosch Institute of Advanced Study, South Africa, id. 49
- Kniazev A. Y., Gvaramadze V. V., Berdnikov L. N., 2015, *MNRAS*, 449, L60
- Kniazev A. Y., Gvaramadze V. V., Berdnikov L. N., 2016, *MNRAS*, 459, 3068
- Kniazev A. Y., Pustilnik S. A., Grebel E. K., Lee H., Pramskij A. G., 2004, *ApJS*, 153, 429
- Kniazev A. Y., Grebel E. K., Pustilnik S. A., Pramskij A. G., Zucker D. B., 2005, *AJ*, 130, 1558
- Kniazev A. Y. et al., 2008, *MNRAS*, 388, 1667
- Kobulnicky H. A., Nordsieck K. H., Burgh E. B., Smith M. P., Percival J. W., Williams T. B., O'Donoghue D., 2003, in Iye M., Moorwood A. F. M., eds, *Proc. SPIE Conf. Ser. Vol. 4841, Instrument Design and Performance for Optical/Infrared Ground-based Telescopes*. SPIE, Bellingham, p. 1634
- Kudritzki R. P., Puls J., Lennon D. J., Venn K. A., Reetz J., Najarro F., McCarthy J. K., Herrero A., 1999, *A&A*, 350, 970
- Lamers H. J. G. L. M., Pauldrach A. W. A., 1991, *A&A*, 244, L5
- Lamers H. J. G. L. M., Snow T. P., Lindholm D. M., 1995, *ApJ*, 455, 269
- Lamers H. J. G. L. M., Cassinelly J. P., 1999, *Introduction to stellar winds*, Cambridge University Press
- Lamers H. J. G. L. M., Nota A., Panagia N., Smith L. J., Langer N., 2001, *ApJ*, 551, 764
- Langer N., 1997, in Nota A., Lamers H., eds, *ASP Conf. Ser. Vol. 120, Luminous Blue Variables: Massive Stars in Transition*. Astron. Soc. Pac., San Francisco, p. 83
- Langer N., 1998, *A&A*, 329, 551
- Langer N., 2012, *ARA&A*, 50, 107
- Lanz T., Hubeny I., 2003, *ApJS*, 146, 417
- Lyubimkov L. S., 1984, *Astrophysics*, 20, 255
- Mahy L., Hutsemékers D., Royer P., Waelkens C., 2016, *A&A*, 594, A94
- Markova N., Puls J., Repolust T., Markov H., 2004, *A&A*, 413, 693
- Marston A. P., 1995, *AJ*, 109, 1839
- Martins F., Plez B., 2006, *A&A*, 457, 637
- Martins F., Hillier D. J., 2012, *A&A*, 545, A95
- Martins F., Schaerer D., Hillier D. J., 2005, *A&A*, 436, 1049
- McLean B. J., Greene G. R., Lattanzi M. G., Pirenne B., 2000, in Manset N., Veillet C., Crabtree D., eds, *ASP Conf. Ser. Vol. 216, Astronomical Data Analysis Software and Systems IX*. Astron. Soc. Pac., San Francisco, p. 145
- Meixner M. et al., 2006, *AJ*, 132, 2268
- Melnick J., 1987, in Khachikian E. E., Fricke K. J., Melnick J., eds, *IAU Symp. 121, Observational Evidence of Activity in Galaxies*. Kluwer Academic Publishers, Dordrecht, p. 545
- Meynet G., Maeder A., 2000, *A&A*, 361, 101
- Mokiem M. R. et al., 2007, *A&A*, 473, 603
- Morrell N. I., Walborn N. R., Fitzpatrick E. L., 1991, *PASP*, 103, 341
- Najarro F., 2001, in de Groot M., Sterken C., eds, *ASP Conf. Ser. Vol. 233, P Cygni 2000: 400 Years of Progress*. Astron. Soc. Pac., San Francisco, p. 133
- Najarro F., Hanson M. M., Puls J., 2011, *A&A*, 535, A32
- Nandy K., Thompson G. I., Morgan D. H., Houziaux L., 1984, *MNRAS*, 210, 131
- Nota A., Livio M., Clampin M., Schulte-Ladbeck R., 1995, *ApJ*, 448, 788
- O'Donoghue D. et al., 2006, *MNRAS*, 372, 151
- Pauldrach A. W. A., Puls J., 1990, *A&A*, 237, 409
- Penny L. R., Gies D. R., 2009, *ApJ*, 700, 844
- Pilbratt G. L. et al., 2010, *A&A*, 518, L1
- Pojmański, G., 2002, *Acta Astron.*, 52, 397
- Puls J., Markova N., Scuderi S., Stanghellini C., Taranova O. G., Burnley A. W., Howarth I. D., 2006, *A&A*, 454, 625
- Puls J. et al., 1996, *A&A*, 305, 171
- Rieke G. H. et al., 2004, *ApJS*, 154, 25
- Rousseau J., Martin N., Prévot L., Rebeiro E., Robin A., Brunet J. P., 1978, *A&AS*, 31, 243
- Russell S. C., Dopita M. A., 1992, *ApJ*, 384, 508
- Sana H. et al., 2012, *Science*, 337, 444
- Sana H. et al., 2013, *A&A*, 550, A107
- Sanduleak N., 1970, *Contribution, La Serena: Cerro Tololo*, 89
- Smartt S. J., Lennon D. J., Kudritzki R. P., Rosales F., Ryans R. S. I., Wright N., 2002, *A&A*, 391, 979
- Smith N., Vink J. S., de Koter A., 2004, *ApJ*, 615, 475
- Smith L. J., Nota A., Pasquali A., Leitherer C., Clampin M., Crowther P. A., 1998, *ApJ*, 503, 278
- Smith Neubig M. M., Bruhweiler F. C., 1999, *AJ*, 117, 2856
- Sota A., Maíz-Apellániz J., Walborn N.R., Alfaro E.J., Barbá R.H., Morrell N.I., Gamen R.C., Arias J.I., 2011, *ApJS*, 139, 24
- Sota A., Maíz-Apellániz J., Morrell N. I., Barbá R. H., Walborn N. R., Gamen R. C., Arias J. I., Alfaro E. J., 2014, *ApJS*, 211, 10
- Steele I. A., Negueruela I., Clark J. S., 1999, *A&AS*, 137, 147
- Šurlan B., Hamann W.-R., Kubát J., Oskinova L. M., Feldmeier A., 2012, *A&A*, 541, A37
- Šurlan B., Hamann W.-R., Aret A., Kubát J., Oskinova L. M., Torres A. F., 2013, *A&A*, 559, A130
- Taylor W. D., Evans C. J., Simón-Díaz S., Sana H., Langer N., Smith N., Smartt S. J., 2014, *MNRAS*, 442, 1483
- Van Genderen A. M., 2001, *A&A*, 366, 508
- Vink J. S., de Koter A., Lamers H. J. G. L. M., 1999, *A&A*, 350, 181
- Vink J. S., de Koter A., Lamers H. J. G. L. M., 2000, *A&A*, 362, 711
- Vink J. S., Brott I., Gräfener G., Langer N., de Koter A., Lennon D. J., 2010, *A&A*, 512, L7
- Wachter S., Mauerhan J.C., van Dyk S.D., Hoard D.W., Kafka S., Morris P.W., 2010, *AJ*, 139, 2330
- Weis K., Bomans D. J., Chu Y.-H., Joner M. D., Smith R. C., 1995, in Pena M., Kurtz S., eds, *Rev. Mex. Astron. Astrofis. Ser. Conf.*, 3, 237
- Weis K., Chu Y.-H., Duschl W. J., Bomans D. J., 1997, *A&A*, 325, 1157
- Zaritsky D., Harris J., Thompson I. B., Grebel E. K., 2004, *AJ*, 128, 1606